Bulletin of Volcanology (2019) 81: 59
https://doi.org/10.1007/s00445-019-1318-5

RESEARCH ARTICLE

The ~ AD 500–700 (Late Classic) El Astillero and El Pedregal volcanoes (Michoacán, Mexico): a new monogenetic cluster in the making?

Patricia Larrea[1,2,3] · Claus Siebe[3] · Erick Juárez-Arriaga[4] · Sergio Salinas[5] · Héctor Ibarra[4] · Harald Böhnel[4]

Received: 28 January 2019 / Accepted: 29 August 2019 / Published online: 13 September 2019

Abstract

The recent identification of Holocene volcanic clusters in small areas within the Michoacán Guanajuato Volcanic Field (MGVF) opens several questions regarding future volcanic hazard assessments in this region. Documenting vent alignments and eruption recurrence intervals within clusters will provide parameters necessary for making temporal and spatial hazard evaluations. Here, we present a possible new case of a small cluster consisting of only two monogenetic volcanoes, El Astillero and El Pedregal located in the ~4400-km^2 Tancítaro-Nueva Italia region in the southwestern part of the MGVF, only 25 km to the south of Paricutin volcano. We determined from paleomagnetic and radiocarbon dating that El Astillero and El Pedregal most likely erupted one after the other between AD 500 and 700 (within the Late Classic period of Mesoamerican archeology). While the eruptions were likely separated by a short period of time, the exact length is difficult to ascertain. After the ~6 years of total estimated eruption duration of the two volcanoes, both together occupied an area of 14.7 km^2 and emitted a dense rock equivalent (DRE) volume of magma of ~0.5 km^3. Notable characteristics of the eruptions include a switch from the explosive activity exclusive of El Astillero (Strombolian) to effusive activity early after the initiation of the El Astillero eruption, a shift in the active vents, and a progressive change in the bulk magma composition from basaltic andesite to andesite throughout the duration of the eruption. This activity first formed the El Astillero scoria cone and tephra deposits followed by its lava field and ended with the emplacement of the El Pedregal viscous lavas. The discovery of pre-Hispanic pottery sherds and obsidian artifacts underneath the El Astillero tephra fallout unambiguously attests to human activities in the area before the eruption. Judging by their eruptive style, the eruptions probably had a limited impact on the small area affected and the surrounding human activities, but the hazard for this area remains since El Astillero and El Pedregal could represent the initial stages of a new cluster that is still in the making. If so, another eruption should be expected in this area again.

Keywords Monogenetic cluster · Holocene · Radiocarbon dating · Paleomagnetic dating · Archeology · Volumetric estimations

Editorial responsibility: C.E.Gregg

Electronic supplementary material The online version of this article (https://doi.org/10.1007/s00445-019-1318-5) contains supplementary material, which is available to authorized users.

✉ Patricia Larrea
plarrea@ing.uchile.cl

[1] Department of Geology and Andean Geothermal Center of Excellence (CEGA), Facultad de Ciencias Físicas y Matemáticas, Universidad de Chile, Plaza Ercilla 803, Santiago, Chile

[2] Department of Geology & Environmental Earth Science, Miami University, 118 Shideler Hall, Oxford 45056, OH, USA

[3] Departamento de Vulcanología, Instituto de Geofísica, Universidad Nacional Autónoma de México, Ciudad Universitaria, Coyoacán, 04510 Ciudad de México, Mexico

[4] Centro de Geociencias, Universidad Nacional Autónoma de México, Blvd. Juriquilla No. 3001, 76230 Querétaro, Mexico

[5] Facultad de Ingeniería, División de Ingeniería en Ciencias de la Tierra, Universidad Nacional Autónoma de México, Ciudad Universitaria, Coyoacán, 04510 Ciudad de México, Mexico

Introduction

Most volcanic fields, regardless of their tectonic setting, exhibit spatial monogenetic vent clustering, likely reflecting structural trends (e.g., faults, joints, and fractures) (Connor 1990; Conway et al. 1998; Connor et al. 2012; Le Corvec et al. 2013; Deligne et al. 2016). Aspects of vent clustering, such as spacing between clusters and spacing between scoria cones within a cluster, have been proposed to correlate with magma reservoir depth and crustal thickness (e.g., Connor 1990; Pérez-López et al. 2011; Le Corvec et al. 2013; Di Traglia et al. 2014). Moreover, spatial clustering of scoria cones has long been recognized (Hasenaka and Carmichael 1985b; Connor 1990); however, the recent (e.g., Guilbaud et al. 2012; Mahgoub et al. 2017a; Mahgoub et al. 2018; Reyes-Guzmán et al. 2018) discovery of temporal clustering opens new and promising avenues of inquiry. The hazard of future activity in monogenetic fields has not yet been adequately evaluated. Smith and Németh (2017) noted the increasing interest in the study of the volcanology, geochemistry, age, structural, and tectonic controls of monogenetic fields in the last decade, due to the need to understand the hazards associated with such monogenetic eruptions and develop well-aimed monitoring strategies, mostly because of the close proximity to population centers.

The Trans-Mexican Volcanic Belt (TMVB) is one of the most complex and active subduction-related volcanic arcs worldwide with ~ 8000 volcanic edifices, and it includes several volcanic fields dominated by monogenetic volcanoes (Fig. 1). Among these fields, the ~ 40,000-km^2 Plio-Quaternary Michoacán-Guanajuato Volcanic Field (MGVF), situated in the west-central part of the TMVB (Fig. 1), is certainly the largest in Mexico, and maybe also in the world (Hasenaka and Carmichael 1985a; Valentine and Connor

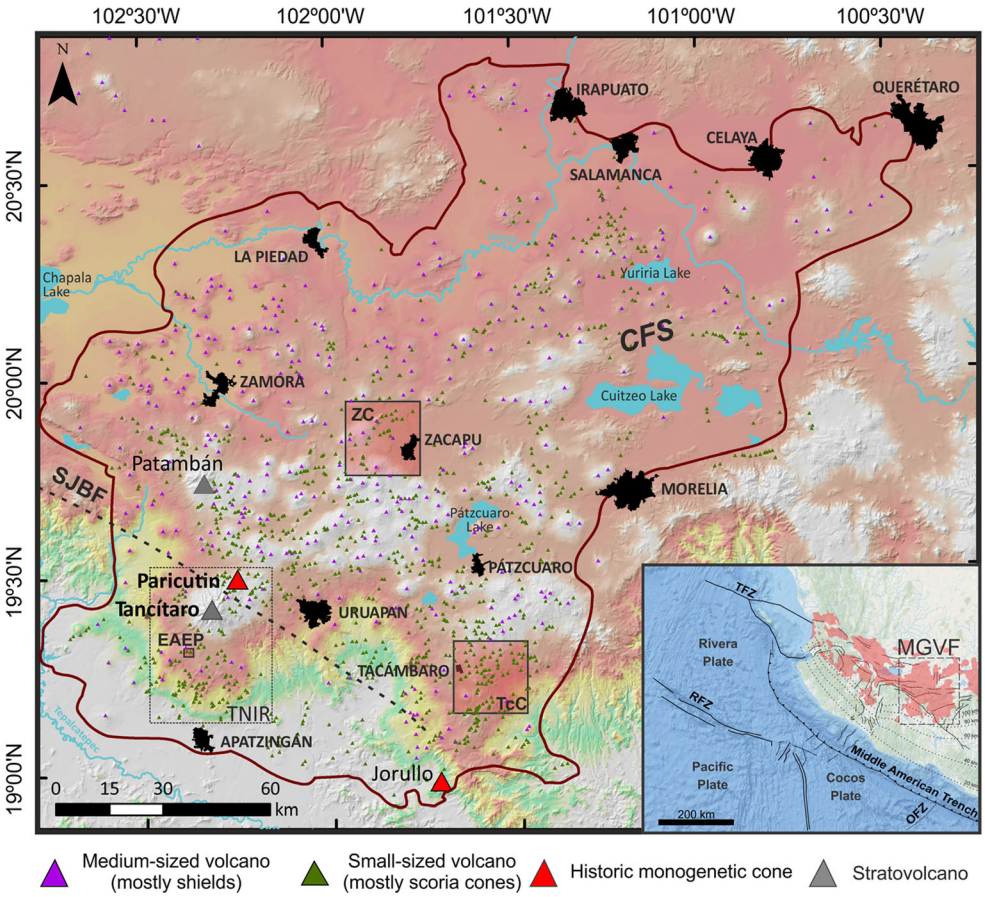

Fig. 1 Digital elevation model of the Michoacán-Guanajuato Volcanic Field (MGVF; outlined in red) showing the location of the El Astillero and El Pedregal volcanoes (EAEP), the Zacapu (ZC) and Tacámbaro clusters (TcC), the historic Paricutin and Jorullo volcanoes, the Tancítaro and Patambán stratovolcanoes, the San Juanico-Buenavista (SJBF) and Cuitzeo (CFS) fault systems, and the Tancítaro-Nueva Italia region (TNIR). The small-sized and medium-sized volcano database modified after Chevrel et al. (2016b) is also plotted (small triangles). The DEM was retrieved from the online 1:50,000 *Relieve Continental* tool, courtesy of INEGI (http://www.beta.inegi.org.mx/temas/mapas/relieve/continental). Inset map shows the general geotectonic map of Mexico with the location of the Trans-Mexican Volcanic Belt (reddish color) and the MGVF. Major fractures zones are TFZ Tamayo Fracture Zone, RFZ Rivera Fracture Zone, OFZ Orozco Fracture Zone. Inferred depth of the subducted Rivera and Cocos plates is also shown

2015). It has a magmatic flux of ~ 800 km^3/Ma (Hasenaka and Carmichael 1985b) and hosts > 1100 scoria cones and associated lava flows (Guilbaud et al. 2012; Mahgoub et al. 2017a), ~ 400 small-to-medium-sized shield volcanoes (Pola et al. 2014; Chevrel et al. 2016a, b; Mahgoub et al. 2017b), ~ 22 phreatomagmatic vents (maars and tuff rings; Kshirsagar et al. 2015, 2016), two extinct stratovolcanoes Tancítaro and Patambán (Ownby et al. 2007; Siebe et al. 2014), as well as ~ 43 domes and isolated lava flows (Mahgoub et al. 2018). Among these eruptive centers within the MGVF are at least 30 that are younger than 25,000 years BP, including the historic eruptions of Jorullo and Paricutin (Luhr and Simkin 1993; Guilbaud et al. 2011; Rasoazanamparany et al. 2016; Larrea et al. 2017, 2019). The eruptive recurrence interval in the MGVF over the past 40 ka has been estimated at $\sim 2 \times 10^{-3}$ events per year, which is significantly higher than the long-term Quaternary average of $\sim 4 \times 10^{-4}$ events per year (Hasenaka and Carmichael 1985b; Valentine and Connor 2015), suggesting that the present time may represent a particularly active phase of this volcanic field. The cause for the concentration of such a large number of monogenetic volcanoes in the MGVF is still poorly understood. Recent studies point to the near-horizontal position of the subducting Cocos plate at a depth of 90–120 km, as the most likely control of the location and areal extent of magmatism over this wide area beneath a ~ 40-km-thick continental crust (Carmichael 2002; Kim et al. 2012; Chevrel et al. 2016a).

Multidisciplinary approaches in the MGVF combining detailed radiocarbon and paleomagnetic dating have revealed that some spatial clusters also represent clusters in time since the different volcanoes comprising each cluster erupted within a brief period of less than 4000 years. The two recently documented clusters occur near the cities of Tacámbaro (Guilbaud et al. 2012; Mahgoub et al. 2017a) and Zacapu (Reyes-Guzmán et al. 2018; Mahgoub et al. 2018), respectively, both along major normal fault zones (Fig. 1). Each of them comprises four monogenetic vents that erupted in a sequence of geologically short time intervals (hundreds to few thousands of years) within a small area (few tens of km^2). The identification of these Holocene clusters in small areas within the MGVF opens several questions in regard to future volcanic hazard assessments in this region. These include the following: Are the magma reservoirs feeding the Holocene clusters still "active" and is a new eruption likely to occur within their surroundings? How long are such clusters active? Will the next monogenetic eruption in the MGVF be a single short-lived isolated eruption, or will it be part of an already existing cluster, or the beginning of a new cluster?

The MGVF region not only presents potential natural hazards, but also has provided an environment conducive to human settlement through pre-historical times. Considering the abundance of Holocene volcanoes, past eruptions must have played an important role influencing pre-Hispanic human development and triggering population migrations in the area (Chevrel et al. 2016b; Siebe et al. 2018). Nomadic prehistoric humans have inhabited the territory of the present State of Michoacán probably since at least 12,000 years BP (Punzo-Díaz and Martínez-Vázquez 2018; Faugere 2006). They started growing corn (*Zea mays*) since at least 3500 years BP (Watts and Bradbury 1982), but the earliest sedentary populations in Michoacán are documented in the Early and Middle Formative periods (2000–300 BC) of Mesoamerican archeology (Beekman 2010). Later, during the Late Formative and Classic periods (300 BC-AD 500/600), small village societies and ceremonial centers appeared across the entire region, a pattern that continued through the Late Classic (AD 500/600–900) and Early/Middle Postclassic (AD 900–1350) with increased population growth. In the Late Postclassic (from AD 1350 onward), the Pátzcuaro lake basin (Fig. 1) became the political core of the Tarascan Empire (Pollard 1993) with urbanization of major settlements, coming to an end in the early 1530s with the Spanish conquest and succeeding decimation of the indigenous population. The impact of volcanic eruptions on the pre-Hispanic populations of Michoacán has never been evaluated due to insufficient archeological and volcanological records. However, the historical eruptions of Jorullo (1759–1774) and Paricutin (1943–1952) revealed the noteworthy social and environmental changes that even small Strombolian eruptions can produce (Luhr and Simkin 1993; Guilbaud et al. 2009). In particular, during the 9 years of the Paricutin eruption, two villages were destroyed, more than 4500 people were mobilized (Nolan 1979; Rees 1979), and 24.8 km^2 of land was buried under lava, and 300 km^2 was covered by > 15 cm of ash fallout (Luhr and Simkin 1993).

In the present multidisciplinary work, we address some of the questions outlined above and present a possible new case of a small cluster consisting of only two monogenetic volcanoes, El Astillero and El Pedregal, near the town of Tancítaro, located 25 km to the south of Paricutin volcano (Figs. 1 and 2). We investigate their age, erupted volumes, and geochemical evolution and report the existence of abundant ancient pottery sherds and obsidian artifacts buried underneath the volcanic products. Furthermore, we establish the sequence of eruption of the two vents, try to shed some light on the conditions that allowed two magmas to be emplaced in close temporal and spatial proximity, and discuss whether another eruption could be expected in this area again in the future.

Geological background and previous works

The Late Holocene El Astillero and El Pedregal monogenetic volcanoes are located in the ~ 4400-km^2 Tancítaro-Nueva Italia region in the southwestern part of the MGVF (Ownby et al. 2011; Fig. 1). This volcanic region is located where the NW-SE trending San Juanico-Buenavista (SJBV) strike-slip fault (Johnson and Harrison 1990; Pacheco et al. 1999)

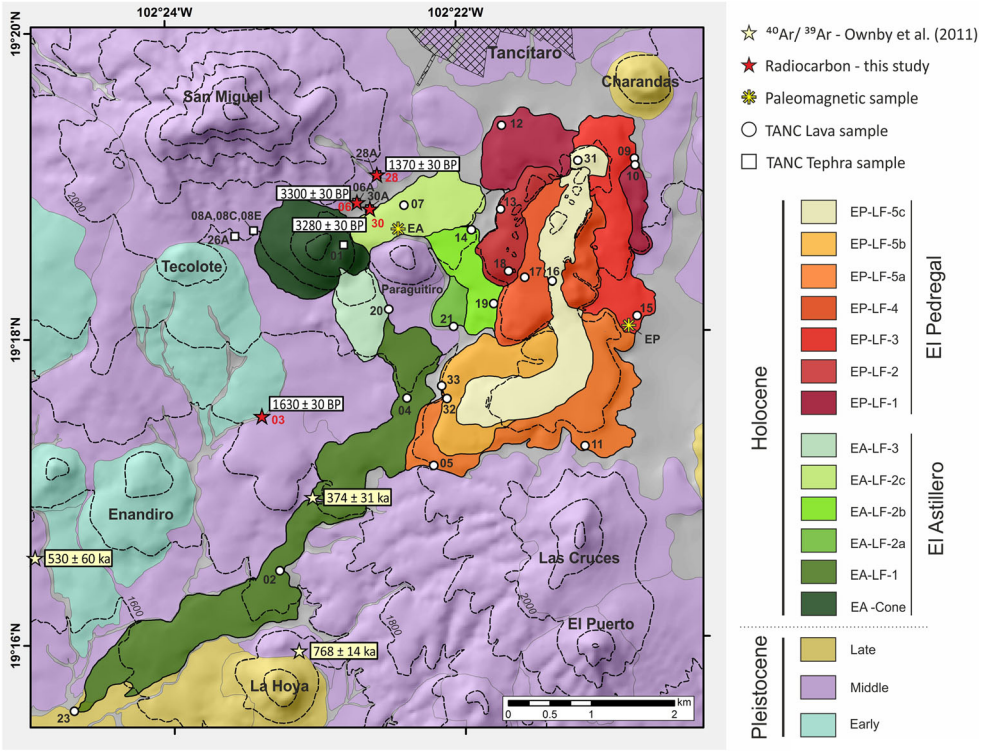

Fig. 2 Digital elevation model and geologic map of El Astillero and El Pedregal volcanoes showing the emplacement sequence of the different lava flows. The locations of the samples collected for radiocarbon (paleosols) and paleomagnetic dating, and geochemical analyses (lavas and tephras) are indicated. Note that sample names have been shortened in the figure to the last two identification digits (e.g., TANC-1801 is referred as 01) for clarity. Digital elevation model (DEM) and topographic map (contour interval 100 m) are from INEGI. $^{40}Ar/^{39}Ar$ ages of older volcanic products dated by Ownby et al. (2011) are also indicated

separates the Michoacán from the Guerrero tectonic block (Fig. 1). The SJVB passes between the Tancítaro and Paricutin volcanoes, being an extension towards the SE of the Cotija half-graben along which numerous volcanic vents are aligned (Hasenaka and Carmichael 1985b; Connor 1987).

The Tancítaro-Nueva Italia volcanic region is constituted by ~ 326 ± 57 km^3 of emitted magma from more than 300 vents, including monogenetic scoria cones and small shields (Morelli et al. 2010), many of which are built on the lower slopes of the extinct andesitic Tancítaro stratovolcano (Fig. 1), the highest mountain (3860 m above sea level) in Michoacán. Volcanic activity in the region dates back to ~ 6 Ma and intensified ~ 1.2 Ma (Ownby et al. 2011). The last volcanic episode is represented by the 1943–1952 historical eruption of Paricutin volcano (Luhr and Simkin 1993; Larrea et al. 2017). Based on $^{40}Ar/^{39}Ar$ dating of clean groundmass separates by Ownby et al. (2007), Tancítaro volcano started forming > 793 ± 22 ka, its last effusive activity occurred at 237 ± 34 ka, and its products represent almost one third of the total magma volume (103 ± 5 km^3) erupted in this region.

Apart from Paricutin and Tancítaro (Ownby et al. 2011; Di Traglia et al. 2014), little is known of the other volcanoes in the Tancítaro-Nueva Italia region. Previous works on selected lavas from the MGVF (Hasenaka and Carmichael 1985a, b, 1987; Ban et al. 1992; Hasenaka 1992; Chesley et al. 2002; Verma and Hasenaka 2004; Johnson et al. 2009, 2010) reported a few whole-rock and isotopic analyses, and K-Ar and $^{40}Ar/^{39}Ar$ ages, from the Tancítaro-Nueva Italia volcanic region. From the El Astillero and El Pedregal volcanoes studied here, a total of six major-and-trace element analyses have been previously reported (Hasenaka 1992; Johnson et al. 2009; Ownby et al. 2011).

Methodology and analytical procedures

During three field campaigns (April–October, 2018) in the study area, we mapped the lava field, measured flow and tephra bed thicknesses, determined stratigraphic relations, collected representative tephra and lava as well as paleosol samples, and cored the interior of lavas exposed at quarries for paleomagnetic studies (Fig. 2). Field mapping was supported by an exploration overflight of the study area by C. Siebe and S. Salinas on the 7-February 2010. Targeted volcanoes were circumnavigated in a CESSNA aircraft at different altitudes and distances on days when atmospheric conditions were optimal in terms of visibility. The resulting geological map of the studied area (Fig. 2), including the limits of the two monogenetic volcanoes and their individual lava flows (LF), was drawn with the aid of a 1:50,000 digital elevation model (DEM), topographic maps, and orthorectified aerial photographs from the *Instituto Nacional de Estadística Geografía e Informática* (INEGI). The basal area of each volcano and the volumes of the emitted individual lava flows were estimated with the aid of ArcGIS® software (see full explanation on Online Resource 1). The estimated DEM-aided volumes for each individual lava flow are reported in Table 1. The Fisher

Table 1 Summary of the El Astillero and El Pedregal eruptive sequence with sampled lava flows and calculated length, average thickness, mean width, mean slope, emplacement time, aspect ratio, exposed surface area, and volume

Volcano	Eruptive sequence	Samples	Length (m)	Average thickness (m)	Mean width (m)	Mean slope (°)	Emplacement time (days)	Aspect ratio	Exposed area (m^2)	DEM-aided calculated volume (km^3)	Total volume (km^3)
El Pedregal	5c	TANC-1816 TANC-1831	4321	30	458	5	31	144	1,693,311	0.022	0.457
	5b	TANC-1832 TANC-1833	4259	50	1205	4	42	85	1,014,970	0.047	
	5a	TANC-1811 TANC-1805	5137	40	803	4	73	128	1,726,952	0.082	
	4	TANC-1817	2481	80	812	9	420	31	1,119,539	0.116	
	3	TANC-1809 TANC-1815	1862	100	563	5	590	19	600,806	0.067	
	2	TANC-1813 TANC-1818	2180	30	506	4	122	73	1,255,596	0.049	
	1	TANC-1810 TANC-1812	1526	50	717	3	308	31	1,021,992	0.074	
El Astillero	3	TANC-1820	1218	50	614	9	130	24	518,379	0.021	0.123
	2c	TANC-1807	1702	20	604	4	19	85	880,988	0.011	
	2b	TANC-1814 TANC-1819	2602	20	568	5	21	130	558,861	0.017	
	2a	TANC-1821	2342	15	489	5	8	156	181,144	0.007	
	1	TANC-1802 TANC-1804 TANC-1823	8066	20	687	5	22	403	3,282,109	0.067	

and Schmincke (1984) nomenclature for types of volcanic activity is used throughout the text for consistency.

Fresh lava and tephra samples were collected spanning the entire eruptive sequence of both volcanoes (see Table I, Online Resource 2). All of the samples were studied macroscopically, and a subset (21 lava and eight tephras) was selected for thin-section preparation and whole-rock geochemical analysis (see details on Online Resource 1). Additionally, four paleosol samples were collected for radiocarbon dating (Figs. 2 and 3; Table 2) from the first 2 cm underlying directly ash fallout deposits (Fig. 3; see sampling details and laboratory methods on Online Resource 1). Moreover, multiple fragments of pre-Hispanic pottery (informally called *tepalcates* by the peasants in central Mexico) and obsidian blades were found within the paleosol underneath the El Astillero ash fallout sampled at location TANC-1830 (Figs. 2 and 3d–f).

Paleomagnetic samples were taken at two active quarries (EA and EP in Fig. 2), one located within El Astillero lava flow 2c (EA-LF-2c) and the second one within El Pedregal lava flow 3 (EP-LF-3). These places were selected because they are the only locations found in the entire lava field where

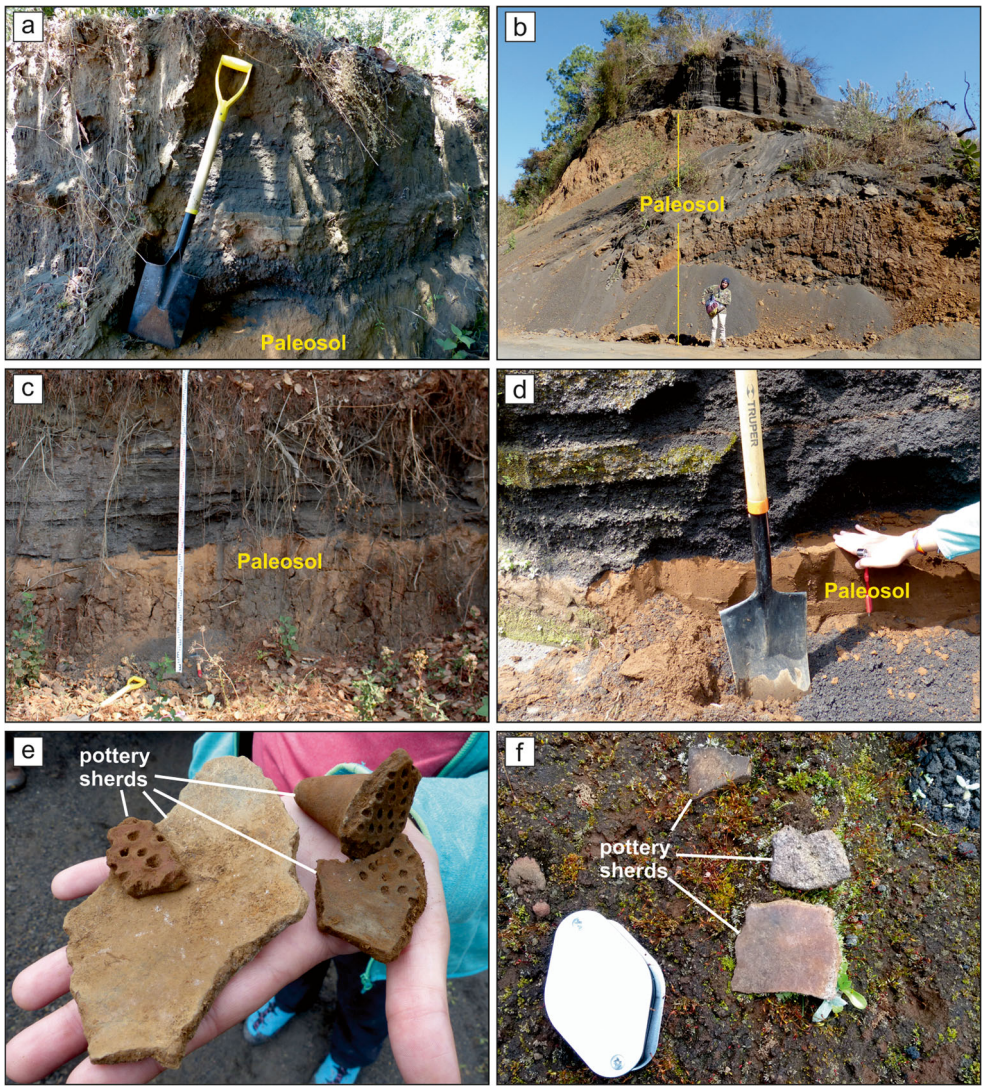

Fig. 3 Photographs showing the outcrops where paleosol samples dated in this study were obtained. **a** Locality TANC-1803 exposing well-bedded ash and scoria-lapilli fallout from El Astillero volcano above paleosol dated at 1630 ± 30 years BP (for size reference shovel is 1 m long). **b** Locality TANC-1806 exposing well-bedded ash and scoria-lapilli fallout from El Astillero volcano above paleosol dated at 3300 ± 30 years BP (for size reference, person is 1.6 m tall). **c** Locality TANC-1828A exposing well-bedded ash and scoria-lapilli fallout from El Astillero volcano above paleosol dated at 1370 ± 30 years BP (zoom in meter for size reference). **d** Locality TANC-1830 exposing well-bedded ash and scoria-lapilli fallout from El Astillero volcano above paleosol dated at 3280 ± 30 years BP (for size reference, shovel is 1 m long as in Fig. 2a). Note that paleosols in **b** and **d** were collected at the same quarry but at different altitudes and stratigraphic positions. Localities are shown in Fig. 2 and radiocarbon dates listed in Table 2. **e**, **f** show photographs of pre-Hispanic pottery sherds found within the paleosol sample TANC-1830 shown in **d** (for size reference, hand is 17 cm long and hand lens is 5.5 × 3.5 cm). Note that the sherds in **d** are parts of a vessel whose floor was grooved or punched with dots

Table 2 Radiocarbon dates of paleosol samples underneath El Astillero ash fallout deposits

Sample name	Coordinates	Altitude (a.s.l.)	Laboratory code	Conventional age (year BP)	∂13C	Calibrated age range (2σ)	Deposit dated	Locality	Reference
TANC-1828	19°19′02.9″ 102°22′33.3″	2063	495,736	1370 ± 30	− 21.8	608–688 cal AD	Upper 2 cm of a > 1-m well-developed paleosol under a 95-cm ash fallout sequence from El Astillero	2 km to the SW of Tancítaro, road to Santa Catarina	This study
TANC-1803	19°17′29.0″ 102°23′22.0″	1820	492,702	1630 ± 30	− 20.8	376–474 cal AD	Upper 2 cm of a > 3-m well-developed paleosol under a 95-cm ash fallout sequence from El Astillero	Santa Catarina village	This study
TANC-1830	19°18′49.1″ 102°22′36.5″	2054	506,219	3280 ± 30	− 18.4	1630–1497 cal BC	Upper 2 cm of a > 1-m well-developed paleosol under a > 1-m ash fallout sequence from El Astillero	El Astillero cone quarry	This study
TANC-1806	19°18′52.0″ 102°22′41.9″	2042	492,703	3300 ± 30	− 19.8	1643–1504 cal BC	Upper 2 cm of a > 6-m well-developed paleosol under a 1.5-m ash fallout sequence from El Astillero	El Astillero cone quarry	This study

the interiors of lava flows are well exposed and not affected by post-emplacement movement. Paleomagnetic analyses were also completed to define rock magnetic properties (O'Reilly 1984; Yu et al. 2001), flow-mean directions and paleointensity determinations, and paleomagnetic dating (e.g., Böhnel et al. 2016; Mahgoub et al. 2017a, b, 2018; Juárez-Arriaga et al. 2018). See Online Resource 3 for details on paleomagnetic sampling details and laboratory methods.

Results

Morphology, eruptive style, stratigraphy, and radiocarbon ages

El Astillero (N 19°18′34.34″N, 102°22′57.24″W, 2230 m.a.s.l.) and El Pedregal (N 19°19′07.08″N, 102°21′04.56″W, 2137 m.a.s.l.) vents are located ~ 3.5 km from each other (Figs. 2 and 4). The morphology of their lava flows is remarkably well preserved and mostly devoid of vegetation, in contrast to older volcanic structures in the surrounding area, which are heavily overgrown by pine forests and avocado orchards (Fig. 4). Both volcanoes were emplaced on an inclined topography sloping 3–9° (GIS-aided) to the SW corresponding to the southwestern flank of Tancítaro volcano (Fig. 1; Table 1). As a result, the longest lava flows from both vents were emplaced downslope in this same direction (Fig. 2). El Astillero was characterized by an initial Strombolian explosive cone-building phase followed by the effusive emission of lava flows, while El Pedregal lacks a cone (i.e., it is a fissure vent) and was purely effusive since neither ash nor spatter deposits were found in its vicinity. If explosive activity had occurred at El Pedregal, El Astillero cone and lava flows would also have been covered by its tephra, which is not the case. The lava flows include aa and blocky surface textures (as defined by Harris et al. 2017) that display lobes, marginal scarps, lateral levees, pressure ridges, and cross-flow ridges (cf. Lipman and Banks 1987, Polacci and Papale 1997, Chevrel et al. 2016b) that can easily be recognized on aerial images allowing the inference of flow trajectories (Fig. 2).

Field mapping and relations allow us to establish the relative chronology of the two vents and their products. Accordingly, El Pedregal is stratigraphically younger than El Astillero as evidenced by the superposition of some of its lava flows (LF-2, LF-4, and LF-5a) over the older El Astillero lava flows (LF-1 and LF-2b). This is apparent on the geologic map (Fig. 2). In this context, it is important to note that paleosols are absent between the different flow units. Paleosol samples were collected within the first two centimeters directly underlying ash fallout deposits from El Astillero volcano at four different locations (Table 2; Figs. 2 and 3a–d). Radiocarbon dating (AMS method) of the bulk organic matter in the paleosols yielded two groups of ages. A younger group of

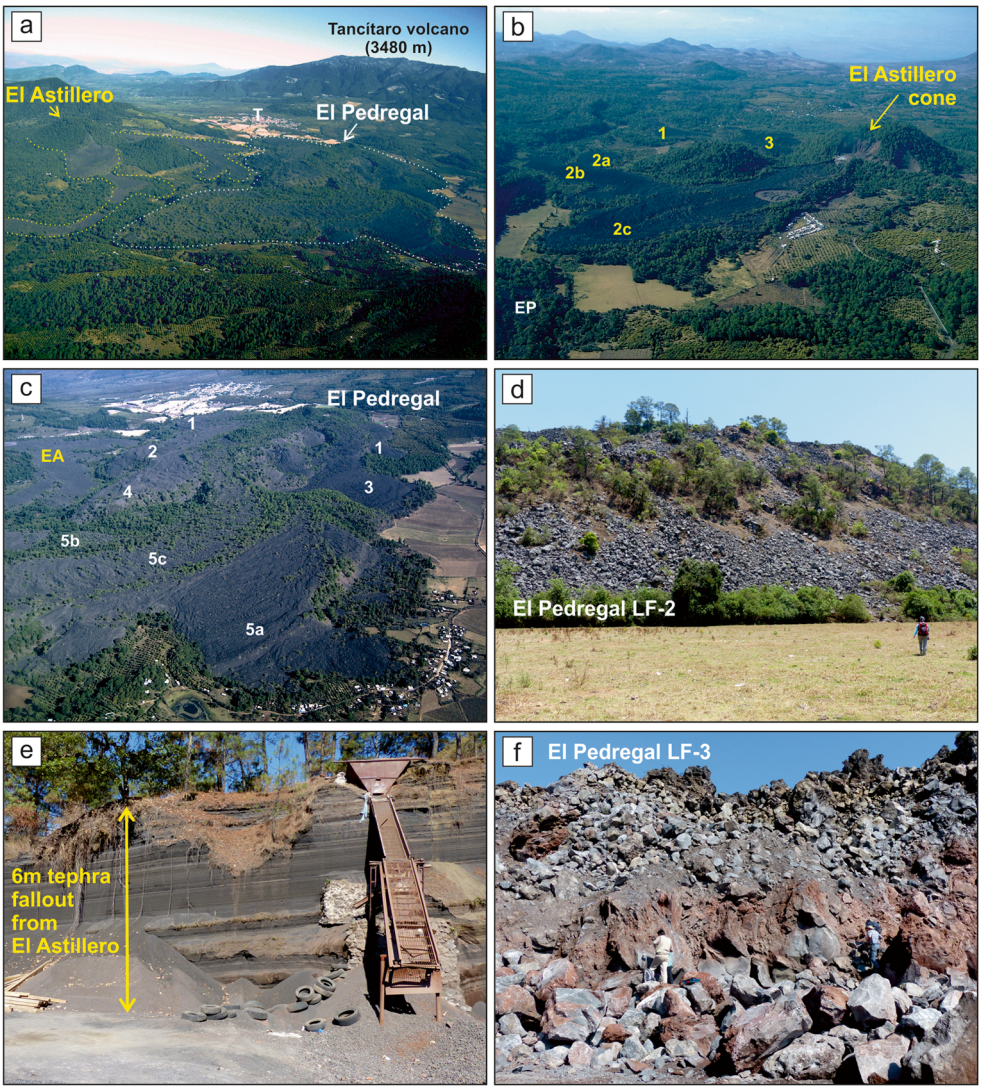

Fig. 4 Features of El Astillero (EA) and El Pedregal (EP) volcanoes (numbers denote lava flows from each volcano as defined in Fig. 2). **a** Aerial view of El Pedregal and El Astillero volcanoes from the south. Tancítaro village (T) is also shown. **b** Aerial view of El Astillero cone and its lava flows from the NE. **c** Aerial view of El Pedregal volcano and its lava field from the SE. **d** Locality of sample TANC-1813 corresponding to El Pedregal lava flow 2 (for size reference, person is 1.65 m tall). **e** Locality TANC-1808 exposing well-bedded ash-and-scoria lapilli fallout from El Astillero cone. **f** Quarry at El Pedregal lava flow 3, where sample TANC-1515 was collected and the paleomagnetic cores from El Pedregal drilled (EP site in Fig. 2). Aerial photos taken by Sergio Salinas on February 07, 2010 (for size reference, person in front is 1.75 m tall)

1370 ± 30 years BP (cal AD 608–688, sample TANC-1828A) and 1630 ± 30 years BP (cal AD 376–474, sample TANC-1803) and an older group of 3300 ± 30 years BP (cal 1643–1504 BC, sample TANC-1806) and 3280 ± 30 years BP (cal 1630–1497 BC, sample TANC-1830).

El Astillero cone has a basal diameter of ~ 1.2 km, a height of 280 m, and a crater diameter of ~ 300 m with a depth of 60 m. It is only slightly eroded and sparsely vegetated. However, it is currently mined for sand and gravel (i.e., ash, lapilli and block) and an abandoned quarry sector is being used as a garbage dump, all of which increases exposure (Fig. 4b). Tephra from El Astillero is best exposed in proximal locations (< 2 km from the vent) to the N, W, and S of the cone, since tephra to the E was buried by its own younger lava flows as well as by flows from the subsequent El Pedregal eruption (Fig. 2). Proximal scoriaceous dark-gray tephra deposits are typically well bedded and comprise millimeter-to-decimeter thick lapilli-and-ash layers with a maximum observed thickness for the entire fallout sequence of ~ 11.5 m at site TANC-1808 (Figs. 2 and 4e). Farther from the cone, widespread surficial erosion and reworking is observed (i.e., lack of original fall-out deposit structure), and the original stratigraphy is only preserved in the lower part of the tephra sequence. El Astillero lavas flowed first towards the E and SE, and after surrounding the preexisting small Paraguitiro edifice (Fig. 2) sharply turned towards the SW, following a ravine which they filled. El Astillero lavas present surface textures that range from rounded clinkery aa to blocky. We identified three distinct flow units formed by five lava flows (Fig. 2); their relative chronology of emplacement was assessed by the contact characteristics between the flows and later confirmed by their compositional differences (Figs. 2 and 4). Lava flow length, measured along the flow axis from the vent to the front, ranges between 1.2 and 8 km and their thickness varies between 15 and 50 m (Table 1). The longest lava flow (8 km long, up to 0.68 km wide, and 20 m thick) was emitted from El Astillero and was also the first to be emplaced. It initially flowed to the SE, but after reaching 1.5 km from the vent

turned towards the SW, following a valley. Subsequent lava flows (EA-LF-2a, 2b, 2c, and EA-LF-3, see Fig. 2) reached shorter distances (< 2.6 km). The thickest lava (EA-LF-3) is also the shortest (1.2 km) with a thickness of 50 m and a lobate form. This was the last emplaced lava from El Astillero.

El Pedregal presents a roughly symmetrical dome-shaped vent (diameter of 420 m with a height of 60 m), open towards the SW marking the outlet of the last lava discharge (EP-LF-5c; Fig. 2). The lava flows are distributed around the summit dome, although most of them flowed towards the SW. They typically display blocky surfaces with single blocks ranging between a few decimeters to several meters in size. Five distinct flow units composed of seven lava flows were identified at El Pedregal from their stratigraphic relations (Fig. 2) and their relative chronology could be determined from their morphologies and contact characteristics, which was later also corroborated by their geochemical composition. Flow lengths range from 1.5 to 5.1 km (measured from vent to front) and their thickness varies between 30 and 100 m (Fig. 4d; Table 1). The youngest lava flow (EP-LF-5c) can be traced from vent to front and, together with EP-LF-5a and 5b, reached longer distances than the other flows due to higher topographical gradients combined with narrow channelized flow close to the vent that broadens downslope forming lobate fronts and butting-up against the earlier formed El Astillero flow (LF-1).

Area, volume estimates, and emplacement duration

With the aid of the GIS-based map, we established the edifice and lava field boundaries, and the basal areas of the volcanoes were estimated at 6.5 km^2 for El Astillero and 8.2 km^2 for El Pedregal, respectively. The estimated total lava volume emitted during the eruption of both volcanoes was 0.58 km^3 (0.123 km^3 for El Astillero and 0.457 km^3 for El Pedregal), and the DEM-aided volume calculated for the small El Astillero cone yielded 0.085 km^3. Volumes of the different lava flows are quite variable (Table 1), and El Pedregal LF-4 (0.11 km^3) is the most voluminous. The above values are not DRE-volumes because empty spaces were not considered. Assuming that 5 vol.% represents void space between the brecciated blocks of lava flow carapaces and basal breccias (cf. Chevrel et al. 2016b), and an additional 5–10 vol.% represents mean volume of vesicles within the lava blocks, the total minimum volume erupted in the form of lava flows (0.58 km^3) from both volcanoes would be ~ 0.5 km^3 DRE.

The well-preserved lava flow surface-morphology of El Astillero and El Pedregal volcanoes allows estimation of their emplacement duration by applying the method of Pinkerton and Wilson (1994) and by following the procedure delineated in Chevrel et al. (2016a). The latter assumes that the different lava flows were not emplaced simultaneously but one after the other. The method of Pinkerton and Wilson (1994) is based on the relationship that exists between the amount of cooling of the lava channel and the final maximum flow-length (assuming a constant lava advance rate). Accordingly, the emplacement time of a lava flow can be estimated by dividing its total volume (DEM-aided calculated volume) by the average volumetric effusion rate (see Table I, Online Resource 4). The effusion rates of the lava flows estimated from the Pinkerton and Wilson (1994) approach range between 1.3 and 35 m^3/s, which if assumed constant, when divided by volume, will give emplacement duration (see Table I, Online Resource 4). Accordingly, the El Astillero lava flow field was emplaced during the course of ~ 200 days, while the El Pedregal field took ~ 1590 days to form, which sums up to a little less than 5 years as the total time for the emplacement of both volcanoes (assuming uninterrupted lava emission).

Petrography and chemical composition

El Astillero and El Pedregal samples are porphyritic with 15–45 vol.% of large crystals (200 μm–3.5 mm) embedded in a holocrystalline to hypocrystalline groundmass (Fig. 5). From here onward, we use the term macrocryst to refer to crystals larger than 200 μm, whereas those smaller than 200 μm are referred to as microcrysts, without petrogenetical significance (cf. Jerram and Martin 2008, and references therein). The macrocryst assemblage, occasionally forming together glomeroporphyritic clusters (Fig. 5c, d), comprises olivine (2–18 vol.%), orthopyroxene (1–3 vol.%), clinopyroxene (1–7 vol.%), and plagioclase (1–20 vol.%). The groundmass (55–85 vol.%) is composed of microcrysts of olivine, feldspars, orthopyroxene, clinopyroxene, and spinel and glass. Most of the lavas are poorly vesiculated, but when present, they show irregular to elongated vesicles (< 30 vol.%) up to 2.5 mm in size. Olivine macrocrysts with orthopyroxene peritectic reaction rims (up to 20 μm; Fig. 5a) and plagioclase macrocrysts are ubiquitous in all samples; however, as the eruption progressed, the lavas became characterized by decreasing olivine and increasing pyroxene contents (Fig. 5a–d). Chromite microcrysts are present as inclusions in most olivine, orthopyroxene, and clinopyroxene macrocrysts in all the lava samples (Fig. 5).

In accordance with the petrographic observations, the eruptive products also show a progressive change in chemical composition throughout the eruptive sequence. The composition of sampled lavas and tephras from El Astillero and El Pedregal ranges from basaltic andesite to andesitic following the TAS classification of Le Bas et al. (1986), in agreement with previously published data (Fig. 6). All volcanic products erupted from El Astillero volcano are exclusively basaltic andesite in composition while El Pedregal is mostly andesitic in composition. The last lava flow erupted by El Pedregal (EP-LF-5c comprising samples TANC-1816 and TANC-1831; Figs. 6

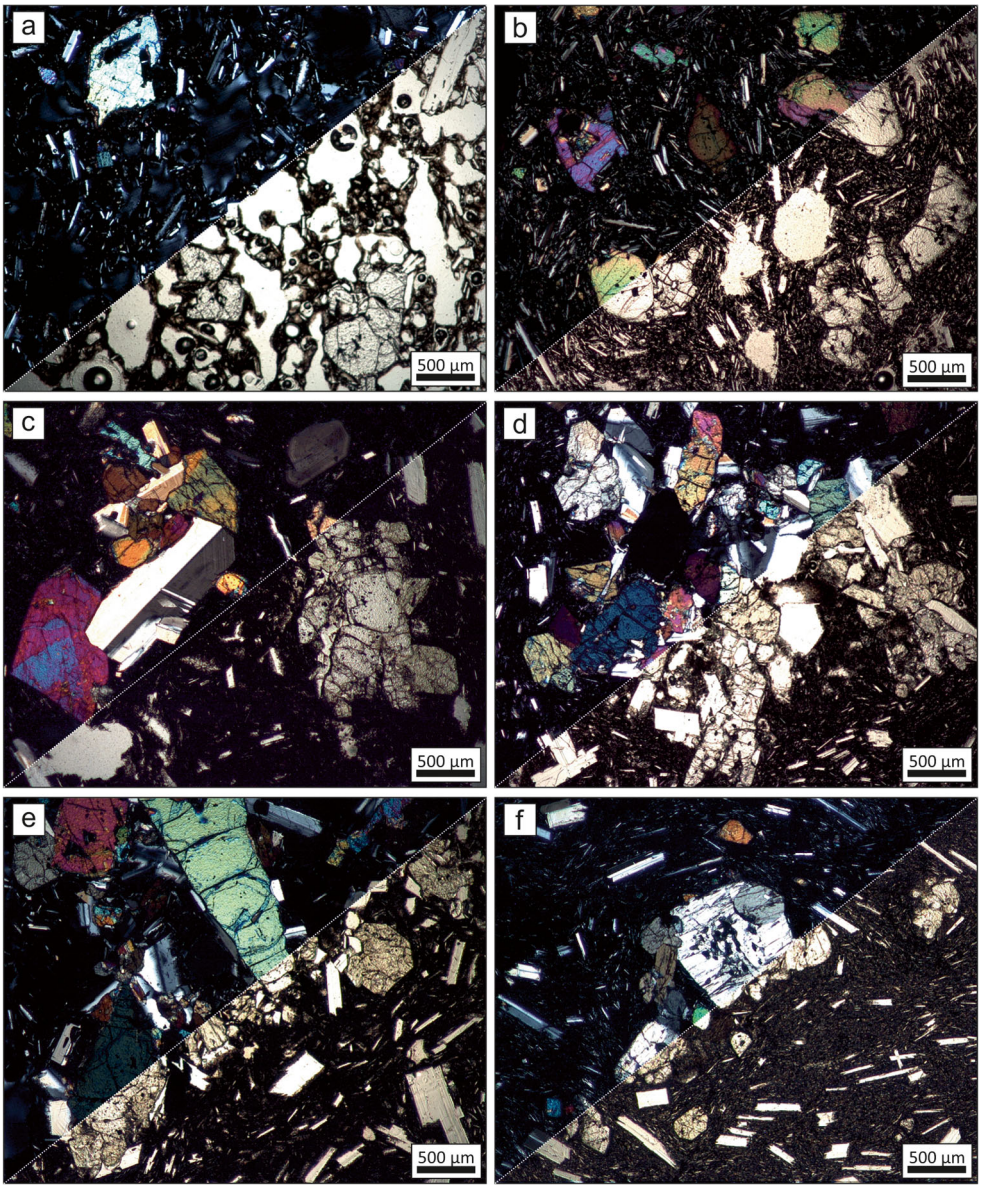

Fig. 5 Representative photomicrographs of El Astillero and El Pedregal volcanic products in plain (upper left) and cross-polarized (lower right) transmitted light. **a** Ol- and Opx-bearing tephra sample from the El Astillero volcano (TANC-1808E); note peritectic rims surrounding Opx. **b** Ol-rich lava sample from El Astillero flow 1 (TANC-1823); note abundance of spinel inclusions in the olivine macrocrysts. **c** Lava sample from El Astillero flow 2c (TANC-1807) with abundant Ol-Cpx-Pl glomerocrysts. **d** Lava sample from El Astillero flow 3 (TANC-1820) with Ol-Opx-Cpx-Pl glomerocrysts. **e** Lava sample from El Pedregal flow 1 (TANC-1810) characterized by large isolated crystals and glomerocrysts. **f** Pyroxene-rich lava sample from El Pedregal flow 5a (TANC-1805)

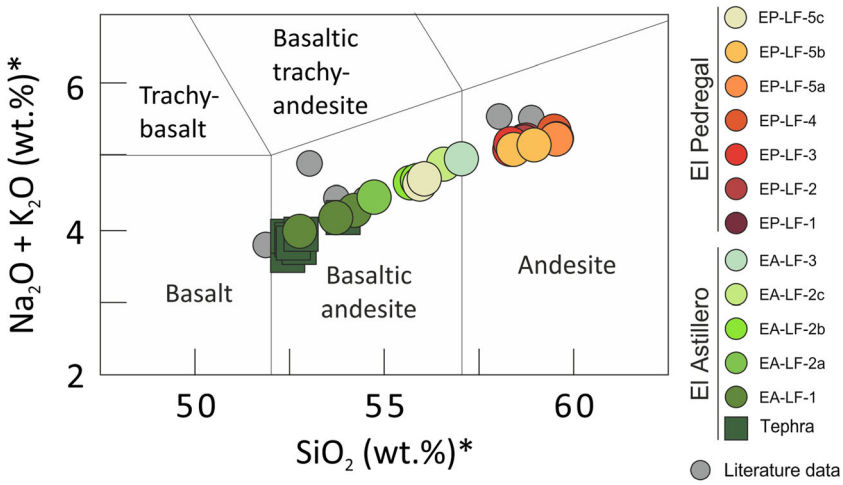

Fig. 6 Total alkalis vs. SiO_2 (TAS) diagram (after Le Bas et al. 1986) for El Astillero and El Pedregal volcanic products. Previously published analyses for El Astillero and El Pedregal (small gray circles) are from Hasenaka (1992), Johnson et al. (2009), and Ownby et al. (2011). *Data normalized to 100% on anhydrous basis

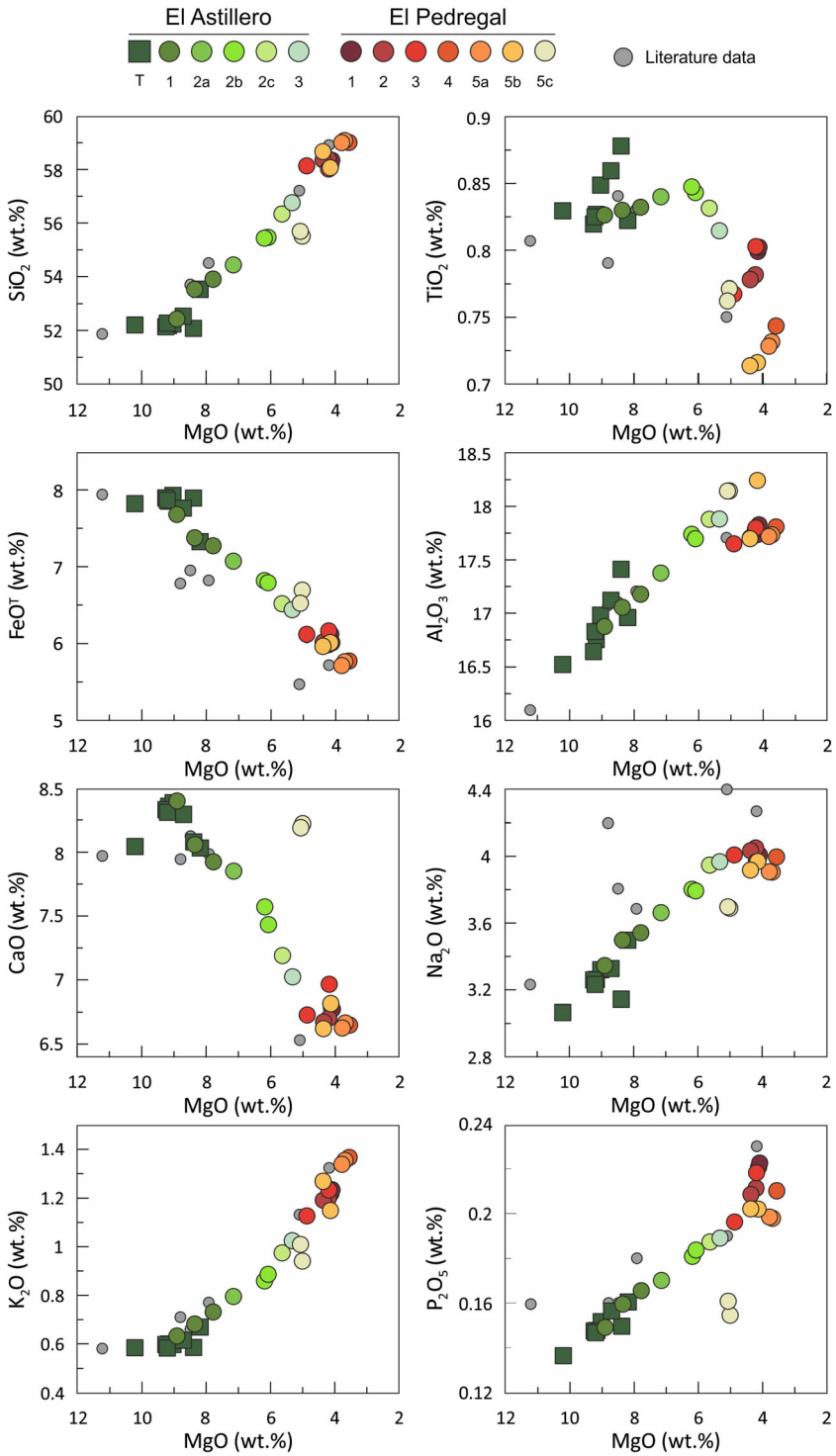

Fig. 7 Major element contents plotted vs. MgO contents for tephras and lava flows from El Astillero and El Pedregal volcanoes. Previously published analyses for El Astillero and El Pedregal (small gray circles) are from Hasenaka (1992), Johnson et al. (2009), and Ownby et al. (2011)

and 7) shows a compositional shift to a more mafic composition, being the only basaltic andesite erupted by this volcano. Taking into account the calculated emitted lava flow volumes (non-DRE) for both volcanoes, andesite is the most voluminous product with 0.435 km^3 (75 vol.%) followed by 0.145 km^3 of basaltic andesite (25 vol.%). Bivariate plots of selected major elements versus MgO (wt.%) are presented in Fig. 7 for El Astillero and El Pedregal volcanic products. Both present a very clear and continuous liquid line of descent, where SiO_2, Al_2O_3, Na_2O, K_2O, and P_2O_5 increase with decreasing MgO, whereas FeO^T and CaO decrease with decreasing MgO, apart from the behavior of the last lava flow emitted as mentioned above. In contrast, TiO_2 shows variable behavior with a clear kink at ~6 wt.% MgO; El Astillero tephras have

Table 3 Rock-magnetic parameters, where M_{rs}/M_s is remanent saturation magnetization/saturation magnetization, H_{cr}/H_c is remanent coercivity/coercivity, and Curie temperature is Tc.

Flow	Site location		Code	Hysteresis analysis		Thermomagnetic analysis
	Latitude (19° N)	Longitude (102° W)		M_{rs}/M_s	H_{cr}/H_c	T_c (°C)
El Astillero	18.688′	22.416	EA6	0.21	1.19	553
			EA13	0.08	1.78	550
			EA17	0.26	1.18	562
El Pedregal	18.035	20.839	EP1	0.11	2.20	512
			EP2	0.11	2.14	572
			EP3	0.08	2.85	525

slight but variable TiO_2 contents (0.82–0.87 wt.%), whereas TiO_2 contents of El Astillero lavas increase until up to ~6% MgO. For samples with MgO < 6% and all El Pedregal lavas, the TiO_2 content decreases with decreasing MgO.

Rock-magnetics, paleomagnetic directions, paleointensities, and paleomagnetic dating

Magnetic hysteresis curves are similar for both lava flows, closing in fields ~300 mT as typical for magnetite or titanomagnetite minerals (Fig. S1 in Online Resource 3). Coercive forces and coercivity and remanence ratios suggest the presence of a mixture of wide grain sizes (Table 3; Online Resource 3). Curie temperature estimates (T_c) yielded values 510 °C < T_c < 580 °C (Fig. S2 in Online Resource 3), indicating the presence of low-Ti titanomagnetite or magnetite (O'Reilly 1984). Chromite inclusions are interpreted to contribute to a very small degree to the magnetism, if at all. A large quantity of chromite, comparable to iron, would be required to produce a measurable effect (Yu et al. 2001). In any case, chromite would record a thermal remanent magnetization (TRM) similar to that of (titano-) magnetite. Rock magnetic properties thus show that the magnetic minerals present in these lava flows are suitable recorders of the paleomagnetic field directions and intensities.

Most alternating field (AF) demagnetization curves are characterized by linear trends towards the origin of the diagram (Zijderveld plots, Fig. S3 in Online Resource 3), indicating the presence of a single magnetization component interpreted to be the primary TRM. Therefore, all demagnetized samples provided stable end-directions. For flow-mean directions, ten cores were drilled distributed over a ~50-m distance in a large and continuous outcrop of EP-LF-3. In the larger quarry of flow EA-LF-2c, the continuity of the massive interior was not as good, but six blocks larger than 3 m and distributed over a distance of ~200 m were sampled for a total of 17 cores. One block with five cores was discarded as it was probably not in situ; one core of EP-LF-3 was similarly rejected. For calculation of mean directions, an outlier test at the 95% confidence level was carried out. Flow average paleomagnetic directions are well defined with small confidence limits α_{95}, providing mean directions for El Astillero at declination (D) = 10.2°, inclination (I) = 35.8°, α_{95} = 3.6°, n = 12 and for El Pedregal at D = 2.6°, I = 35.6°, α_{95} = 2.1°, n = 9 (Fig. 8). While these directions are similar, the F-test indicates that they do indeed not belong to a common distribution. El Pedregal should therefore have erupted at least 50 years after El Astillero to record a statistically different direction, based on the typical secular variation rate around 0.1[a]/year, as obtained by Mahgoub et al. (2019) from the Mexican volcanic belt.

Paleointensity experiments were carried out on 16 samples (10 of El Astillero and 6 of El Pedregal; Table 4). Figure 9 shows representative Arai plots of two accepted samples,

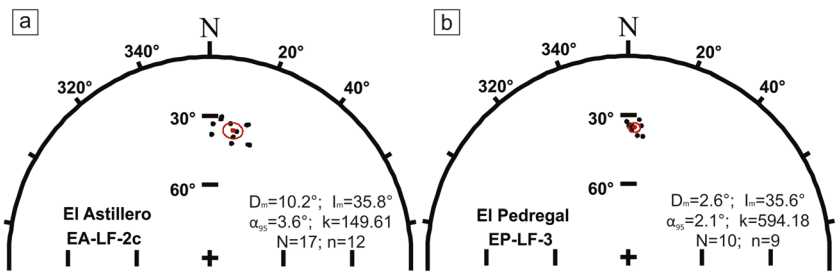

Fig. 8 Equal area projection of paleomagnetic ChRM directions (black dots) and flow-mean directions (red dots) with 95% confidence angles, k precision parameter, *N* total number of samples measured, *n* number of samples used in the calculation of the flow-mean direction for **a** El Astillero lava flow 2c and **b** El Pedregal lava flow 3

Table 4 The IZZI-Thellier and IZZI-Microwave paleointensity, results and associated statistics. *N* – number of points included in the linear best-fit; *T* minimum and maximum temperature used to determine the paleointensity, *P* minimum and maximum power used to determine the paleointensity, β the ratio of standard error of the slope of the selected segment in the Arai plot to absolute value of the slope, *f* fraction of the NRM used for best-fit, *q* quality factor, *MADanc* anchored maximum angular deviation, α angular difference between anchored and non-anchored best solution, *δCK* relative check error, *δpal* cumulative check difference, *PI* paleointensity, *s.d.* standard deviation, *Quality* the quality of the obtained paleointensity data with the two default criteria: classes A and B. The analysis was done using ThellierTool4.22 software (Leonhardt et al. 2004)

Sample	Number	T (°C)	β	f	q	MAD_{anc} (°)	α (°)	δCK (%)	δpal (100%)	PI	s.d. (μT)	Class
El Astillero												
EA6	13	0–550	0.03	0.81	11.8	2.1	1.3	3.0	6.5	45.76	1.54	B
EA13	13	0–550	0.02	0.72	29.5	1.3	1.7	2.6	3.8	47.01	0.93	A
EA14	12	0–530	0.03	0.56	15.9	1.4	2.1	4.0	3.7	49.13	1.32	A
EA17	13	0–550	0.03	0.76	18.1	1.4	0.5	1.9	4.2	47.54	1.54	A
		P (W)										
EA10–1	9	0–60	0.02	0.69	20.47	0.85	0.5	3.6	9.46	38.98	0.87	B
EA10–2	6	0–60	0.05	0.47	6.22	1.01	2.2	2.9	9.99	45.24	2.34	B
EA10–3	7	0–60	0.05	0.49	5.61	2.17	4.5	2.16	6.50	43.17	2.16	B
EA10–5	5	0–50	0.01	0.89	14.77	0.38	0.3	6.38	7.05	36.44	0.59	B
EA13–2	5	0–60	0.01	0.64	47.8	0.60	1.0	2.41	4.94	50.69	0.34	A
Mean										44.88	4.65	
El Pedregal												
		T (°C)										
EP1	10	0–500	0.07	0.38	3.9	1.1	0.6	3.1	8.9	38.47	2.76	B
EP2	8	0–400	0.08	0.38	3.6	1.7	2.4	6.8	4.7	64.42	5.64	B
EP3	5	400–500	0.02	0.55	14.5	1.3	1.5	5.4	5.4	49.18	1.00	B
		P (W)										
EP1–2	6	0–60	0.06	0.64	7.02	2.69	4.3	1.99	4.52	35.51	2.25	A
EP3–3	5	0–80	0.04	0.88	10.88	0.84	0.6	4.92	6.64	46.28	1.94	B
Mean										42.36	6.43	

together with their orthogonal vector plots. Fourteen samples passed the acceptance criteria (Table S4 in Online Resource 3), resulting in an average for El Astillero of 44.88 ± 4.65 μT and for El Pedregal of 42.36 ± 6.43 μT. One El Pedregal sample with a high PI of 64 μT was excluded as an outlier.

Flow mean directions and intensities were used as input data for paleomagnetic dating (Pavón-Carrasco et al. 2014), within a time interval from AD 0–1550 for both lava flows. This interval is defined by the oldest possible ^{14}C age of El Astillero and the Spanish conquest. Resulting probability

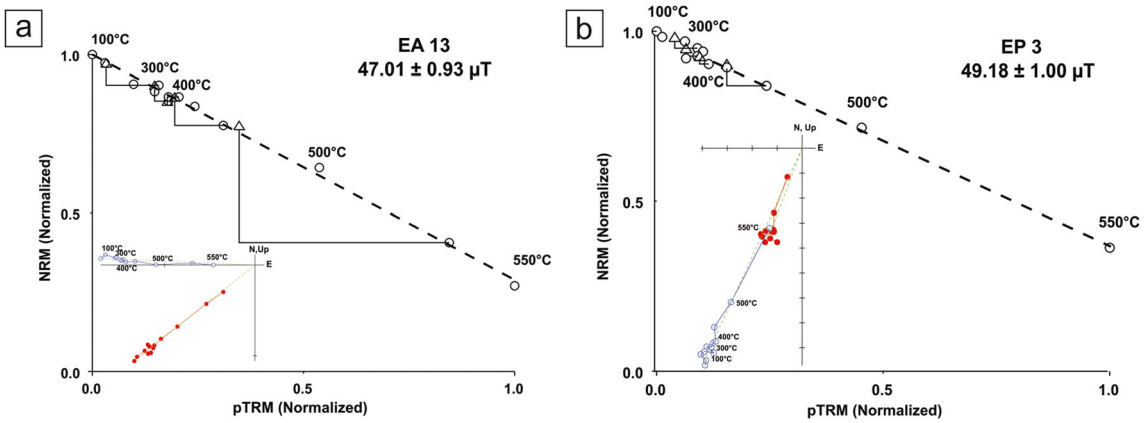

Fig. 9 Examples of paleointensity (Arai) plots for the **a** El Astillero and **b** El Pedregal lava flows, obtained by the IZZI-Thellier protocol (Tauxe and Staudigel 2004). Paleointensity results and orthogonal vector plots (insets). NRM and pTRM data are normalized. NRM vs. pTRM data are shown as circles, with best-fit lines. pTRM checks are shown as triangles and some labels temperatures steps are also indicated. The analyses were carried out using ThellierTool4.22 software (Leonhardt et al. 2004)

density curves are shown in Fig. 10 (further details in Fig. S5 in Online Resource 3) and defines for El Astillero two possible age intervals of AD 40–200 and AD 600–680, with the second one correlating well with the youngest C^{14} age (Fig. 10a). This good agreement validates the paleomagnetic dating method, as already proven recently by Böhnel et al. (2016), Mahgoub et al. (2017a, b, 2018), and Juárez-Arriaga et al. (2018) for other Mexican volcanoes. The older age of AD 40–200 is excluded because of the archeological context (see "Discussion" below). The El Pedregal lava flow provides as well two paleomagnetic age ranges of AD 50–290 and AD 500–700 (Fig. 10b), and here, we exclude the older age as well, as this flow is stratigraphically younger than El Astillero. The age of AD 500–700 is very similar to that of El Astillero lava flow and thus supports a (near-) coeval emplacement of these lava flows. Paleomagnetic dating thus restricts the ^{14}C age range of El Astillero towards younger ages, reducing the uncertainty to 60 years, and allows for a maximum time lag of El Pedregal flow emplacement of 90 years, if the paleomagnetic ages are used for calculation.

Discussion

Are El Astillero and El Pedregal "twins" or "siblings"?

According to the C^{14} ages obtained in the four dated paleosols located below the fallout tephras from El Astillero volcano (Fig. 2; Table 2), two possible paleosol age ranges can be

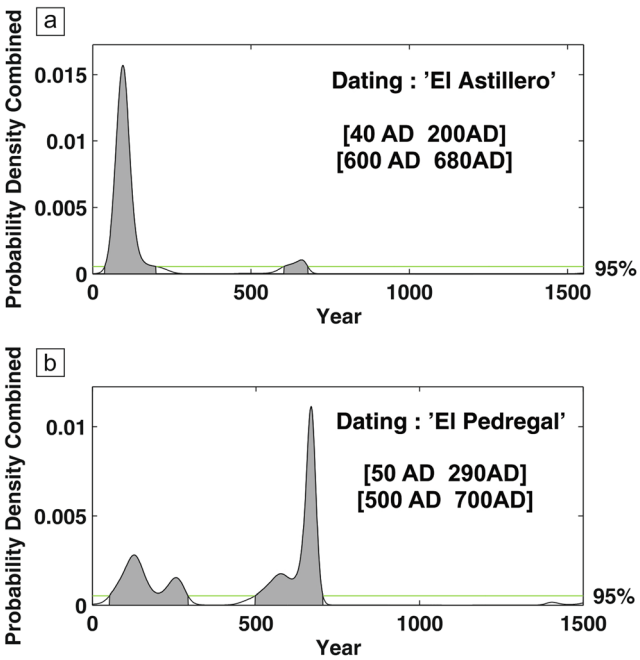

Fig. 10 Paleomagnetic dating of El Astillero and El Pedregal lava flows. Probability density curves are shown with shaded areas below them where surpassing the 95% threshold levels (Pavón-Carrasco et al. 2014)

recognized: a younger (AD 376–688) and an older (1630 to 1530 BC) range. However, thanks to the assortment of *tepalcates* found within the paleosol sampled at locality TAN-1830, which includes a few pottery sherds from vessels characterized by a floor grooved or punched with dots (Fig. 3e, f), we can shed light on this age discrepancy. According to Arnauld et al. (1993) this type of ornamentation has been identified in the archeological complex of Las Lomas in the western part of the Zacapu lacustrine basin (located 80 km to the NE, see Fig. 1), where it has been radiocarbon dated and found to be diagnostic (Gregory Pereyra, pers. comm., November 11, 2018) for the Early Classic period of Michoacán archeology spanning from AD 0 to AD 550. Although the appearance of this ornamentation in the Tancítaro area could have started some years before and/or after its appearance at the Las Lomas archeological site, its occurrence underneath the El Astillero ash is inconsistent with the older age range (1630–1530 BC). In contrast, the younger range (AD 376–688) overlaps partly with the time range of occurrence (AD 0–550) of the diagnostic floor-punched *tepalcates* covered by the El Astillero tephra. Hence, the younger range (AD 376–688) is proposed here as the most likely age for the eruption of El Astillero volcano.

Furthermore, the paleomagnetic dating method yielded most likely age ranges of AD 620–680 for El Astillero and of AD 470–710 for El Pedregal, respectively.

As outlined above, we have no doubt that El Astillero erupted before El Pedregal and that both are petrogenetically closely related. A question that needs to be answered is thus whether they were born during the same fissure eruption, one immediately after the other, and should hence be regarded as contemporaneous twins, or whether sufficient time (decades to a few centuries) elapsed between both eruptions, to rather consider them as separate siblings. In this respect, the paleomagnetic study sheds some light, since it revealed the near-contemporariness of El Astillero and El Pedregal eruptions based on the measured paleomagnetic directions and intensities. Moreover, the paleomagnetic dating has also confirmed the relative chronology established previously for both volcanoes by stratigraphic means. El Pedregal being younger than El Astillero is also in accordance with the progressive geochemical variation of the erupted products, starting with the more primitive basaltic andesite El Astillero tephra and lavas and gradually evolving in time towards the high silica andesite compositions of El Pedregal's succession of lavas. An exception to this general trend is the very last erupted lava flow from El Pedregal (EP-LF-5c) that shows an intermediate composition similar to the most evolved El Astillero magmas. This behavior was also observed in a recent study of Paricutin volcano, where the last erupted lava flow similarly showed a more primitive composition (Larrea et al. 2019).

From all of the above, it seems safe to say that El Astillero and El Pedregal probably erupted between AD 500 and AD

700 (within the Late Classic period of the Mesoamerican archeological time scale), one after the other, and that both eruptions were likely separated by a short period of time, the exact length of which is difficult to ascertain (the pause might have taken a few months, but definitely not more than a few decades). Although it is difficult to conclude beyond doubts whether these two volcanoes should be either regarded as twins or rather as siblings, we are more inclined to favor the second analogy, since our paleomagnetic dating efforts suggest a short pause in activity between the two eruptions.

In summary, the eruption of El Astillero probably started along an ENE-WSW-oriented fissure with Strombolian activity and accompanying intense ash fallout from a pulsating eruptive column, forming rapidly a scoria cone during the first weeks, as also described from other scoria cones of the MGVF (e.g., Paricutin historic eruption; Foshag and González-Reyna 1956, Luhr and Simkin 1993). These initial tephra fallout deposits are best exposed at proximal locations (< 2 km from the cone) to the N, W, and SW of the vent (Fig. 2); at farther distances, fallout deposits quickly become smaller in grain size (mostly fine ash), thin out, and display cross-bedding due to erosional reworking. The explosive activity largely came to an end when the first lava flow emanated from El Astillero, since late fallout deposits were not found, neither covering nor inter-bedded within the lava sequence. The discharge of the first lava flow from El Astillero initiated at the SE base of the scoria cone (Fig. 2). From there, it first flowed 2 km towards the SE until it abruptly changed its direction by 90°, when it became channelized towards the SW along a major ravine draining the upper slopes of Tancítaro stratovolcano. This lava flow reached a distance of ~ 8 km and is not only the longest, but also the most mafic. Afterwards, a new effusive vent opened at the eastern base of the cone, producing subsequently El Astillero lava flows EA-LF-2a, 2b, and 2c. The last lava emitted from El Astillero (EA-LF-3) was produced by the reactivation of the SW vent. After the cessation of El Astillero activity, and presumably after a geologically negligible pause (months to few decades), volcanic activity resumed with the opening of a new effusive vent (El Pedregal dome) located ~ 3.5 km to the ENE of El Astillero scoria cone. Although the cause of this shift is unknown, one potential explanation could be the existence of a structural lineament (e.g., a normal fault) that favored this magma shift and the formation of this younger El Pedregal vent. After its initial opening, abundant and continuous lava flows were emitted and distributed around the dome-shaped vent forming the El Pedregal lava flows EP-LF-1, 2, 3, 4, 5a, 5b, and 5c, until lava emission ceased abruptly bringing the formation of El Pedregal volcano to its end. These viscous lavas flowed mostly to the south (Fig. 2), and their total volume (~ 0.5 km^3) is almost three times larger than the total volume (~ 0.2 km^3) emitted from El Astillero, including the volume of its cone.

The eruptive sequence described above records a relatively abrupt change from an explosive Strombolian to an effusive eruptive style accompanied by a progressive change in the bulk magma composition, evolving from basaltic andesite with a SiO_2 content of ~ 52 wt.% to andesitic with slightly less than 60 wt.% SiO_2 (Fig. 6). As previously noted at Paricutin (Larrea et al. 2017), the case of the El Astillero and El Pedregal eruptions display a somewhat unexpected behavior, since the most primitive magmas (initial tephras from El Astillero) are also the ones related to the most explosive activity. However, Smith and Németh (2017) suggested that the eruptive style in small-volume monogenetic volcanoes strongly depends on parameters such as magmatic volatile content, magma composition and viscosity, and other environmental factors (e.g., basement structures, presence and proportion of external water, and host sediment physical conditions). Therefore, the magma pre-eruptive volatile content and the degassing mechanism, which depends on magma ascent rates and the relative permeabilities of magma and wall rock, were key factors (e.g., Parfitt and Wilson 1995; Cashman 2004; Larrea et al. 2017) controlling the explosive activity of the El Astillero and El Pedregal eruptions. In this case, the change from explosive activity to effusive activity probably took place when slow magma ascent rates and stagnation accompanied by crystallization (Cashman 2004; Cervantes and Wallace 2003) allowed extensive degassing of the remaining El Astillero magma. As a result, the subsequent El Pedregal eruption was purely effusive producing largely degassed lavas allowing the emplacement of more viscous, thicker, and shorter lavas compared to those of the El Astillero lava field.

El Astillero and El Pedregal volcanoes: a monogenetic cluster in the making?

Recent volcanological studies near the small cities of Tacámbaro (Mahgoub et al. 2017a) and Zacapu (Reyes-Guzmán et al. 2018; Mahgoub et al. 2018), both within the MGVF, have led to the discovery of two Late Holocene enigmatic monogenetic volcano clusters. Each consists of four vents that erupted in close proximity to each other within a time period encompassing less than 4000 years. Both initiated with Strombolian activity building first a basaltic andesite scoria cone and associated lava flows (Mahgoub et al. 2017a; Reyes-Guzmán et al. 2018). Subsequently, after periods of repose, each lasting several hundred years, nearby vents erupted producing additional silicic andesite lava flows in an effusive fashion (Mahgoub et al. 2017a, Reyes-Guzmán et al. 2018). In this context, and given the similarities between our case and those of Tacámbaro and Zacapu (cf. Mahgoub et al. 2017a; Reyes-Guzmán et al. 2018) in regard to compositional trends (basaltic to andesitic), erupted volumes, and eruptive styles (Strombolian, followed by effusive activity), we wonder whether El Astillero and El Pedregal could

together represent the initial stages of a new cluster that is still in the making. If so, a remnant batch of degassed crystal-rich magma might still be residing in the upper crust underneath the area waiting to become remobilized by a new injection of mafic magma rising from the mantle. If true, and given the pattern displayed by the Tacámbaro and Zacapu clusters, a new high-silica andesite effusive eruption should be expected in the southern Tancítaro area in the future. Although such a scenario is highly speculative, it represents a line of investigation worth being pursued by geophysical and geochemical means in the future.

Impact of the eruption and archeological implications

Considering the small volume emitted (~ 0.5 km^3) and area covered (14.7 km^2) by its products, as well as the predominance of effusive relative to explosive style of activity of the El Astillero and El Pedregal volcanoes, it seems that their eruptions probably had a relatively localized impact on their surroundings. Before the eruption, this zone was likely covered by a mixed pine and oak forest, similar to the woods currently encountered in the nearby protected areas of the Tancítaro National Park, which has so far been spared from the otherwise extensive replacement by avocado orchards. The existence of pre-Hispanic pottery sherds and obsidian artifacts underneath the tephra fallout deposits from El Astillero unambiguously attest to human activities in the area before the eruption. Future archeological excavations should reveal more about the exact nature and extent of the human occupation. If small hamlets existed, these were probably abandoned as a consequence of the eruption, and those lying in flow paths buried. Unlike other archeological sites in Michoacán such as Malpaís Prieto in the western Zacapu lacustrine basin (Michelet 1993, 1998, Reyes-Guzmán et al. 2018, Pereira and Padilla-Gutiérrez 2018) and Angamuco in the eastern Pátzcuaro basin (Fisher and Leisz 2013; Fisher et al. 2017; Ramírez-Uribe 2017), the young El Astillero and El Pedregal lava flows do not show obvious evidence of re-occupation and settlement on the lavas. However, archeological information in Michoacán is still sparse (Pollard 2011) and more intensive excavations in the future should reveal additional information that will shed light on the role that these eruptions played in the development of ancient societies and their migrations in this region.

Comparison with other volcanoes in the MGVF and future hazards

The monogenetic eruptions of El Astillero and El Pedregal have differences and similarities when compared to other monogenetic eruptions in the MGVF, which includes a large variety of landforms and sizes (e.g., scoria cones, maars, domes, shields, etc.; Hasenaka and Carmichael 1985b). Notable characteristics of the El Astillero and El Pedregal eruptions include a variation in the importance of effusive relative to explosive activity early after the initiation of the El Astillero eruption, a shift in the location of active vents, and a progressive change in the bulk magma composition throughout the duration of the eruption.

After the course of probably not more than 6 years, the new volcanoes occupied an area of 14.7 km^2 and emitted ~ 0.5 km^3 (DRE) of magma. If compared with other known monogenetic volcanoes in the MGVF, El Astillero and El Pedregal together covered only half of the area and emitted one third of the volume of the 9-year long Paricutin eruption; however, it is comparable in size and volume to the 15-year long Jorullo eruption, which covered a much smaller area (~ 11 km^2) with only ~ 0.35 km^3 (DRE) of magma (Rowland et al. 2003, Guilbaud et al. 2011, Rasoazanamparany et al. 2016). However, most of the 114 Quaternary volcanoes (Early Pleistocene to Holocene) identified in the 690-km^2 Tacámbaro-Puruarán area involved small volumes (< 0.5 km^3 DRE) and areas (Guilbaud et al. 2012), being similar to the volcanoes described here. Similarly, in the 395-km^2 western Zacapu lacustrine basin, 47 Quaternary volcanoes were emplaced in the last 2.1 Ma, most of them erupting volumes < 0.5 km^3 DRE. Thus, the systems considered here could be considered typical in terms of size, covered area, erupted volumes, and eruptive styles for monogenetic activity of the region.

Conclusion

The recent identification of Holocene clusters in small areas within the MGVF (Reyes-Guzmán et al. 2018; Mahgoub et al. 2017a, 2018) opens several questions regarding future volcanic hazard assessments in this region. Documenting the eruptive recurrence intervals within clusters, as well as the prevalence of vent alignments, thus provides input parameters necessary for both the temporal and spatial aspects of volcanic hazard assessment. The occurrence and longevity of clusters is ultimately related to magma supply and regional and local stress fields that control magma ascent (Valentine and Connor 2015; Martí et al. 2016); thus, the location of active clusters can migrate with time in response to changes in tectonics and, potentially, melt production and magma flux. Nevertheless, for clusters with eruptive recurrence intervals that are short with respect to the timescale for significant stress field changes, new vents may be expected to occur within currently active clusters (Deligne et al. 2016). We here provide a multidisciplinary approach involving field mapping, physical volcanology, geochemistry, paleomagnetism, and archeology to place the timing and duration of activity at nascent monogenetic systems. Therefore, detailed studies of a wide variety of monogenetic volcanoes occurring in the MGVF,

similar to that presented here, could allow constraints to be placed on a range of possible future scenarios, including potential relationships between eruption magnitude, size, and severity of affected areas.

Acknowledgments Jorge Escalante supported rock magnetic measurements and Emilio Nava supported the functionality of the computer network in the paleomagnetic laboratory. Capitán Fernando Valencia is thanked for skillful and safe flights over the study area. Gregory Pereira (Sorbonne University, Paris) kindly provided advice in regard to archeological questions. The personnel of *Protección Civil* and Miguel Equihua (*Desarrollo Rural y Ecología*) of the municipality of Tancítaro are thanked for always being kind and helpful in coordinating fieldwork activities. Associate Editor Christopher Gregg and Executive Editor Andrew Harris are warmly thanked for comments, suggestions, and editorial handling; Karoly Nemeth and one anonymous reviewer are thankfully acknowledged for their constructive reviews, which led to great improvement of the manuscript.

Funding information This work was supported by Consejo Nacional de Ciencia y Tecnología (CONACyT-167231) and Dirección General de Asuntos del Personal Académico (UNAM-DGAPA IN-103618) granted to C. Siebe. Patricia Larrea was supported by UNAM-DGAPA postdoctoral fellowship (2018-2019).

References

Arnauld C, Carot P, Fauvet-Berthelot MF (1993) Arqueología de Las Lomas en la cuenca lacustre de Zacapu, Michoacán, México. Céntre d'Études Mexicaines et Centroaméricaines, México. Cuadernos de Estudios Michoacanos 5, 230 pp

Ban M, Hasenaka T, Delgado-Granados H, Takaoka N (1992) K-Ar ages of lavas from shield volcanoes in the Michoacan-Guanajuato volcanic field, Mexico. Geofis Int 31(4):467–473

Beekman CR (2010) Recent research in western Mexican archaeology. J Archaeol Res 18:41–109

Böhnel H, Pavon-Carrasco FJ, Sieron K, Mahgoub AN (2016) Palaeomagnetic dating of two recent lava flows from Ceboruco volcano, western Mexico. Geophys J Int 207:1203–1215

Carmichael ISE (2002) The andesite aqueduct: perspectives on the evolution of the intermediate magmatism in west-central (105°-99°W) Mexico. Contrib Mineral Petrol 143(6):641–663

Cashman KV (2004) Volatile controls on magma ascent and eruption, in The State of the Planet: Frontiers and Challenges in Geophysics (eds R.S.J. Sparks and C.J. Hawkesworth), American Geophysical Union, Washington, D.C. doi:https://doi.org/10.1029/150GM10

Cervantes P, Wallace P (2003) Magma degassing and basaltic eruption styles: a case study of 2000 year BP Xitle volcano in Central Mexico. J Volcanol Geotherm Res 120:249–270

Chesley J, Ruiz J, Righter K, Ferrari L, Gómez-Tuena A (2002) Source contamination versus assimilation: an example from the Trans-Mexican Volcanic Arc. Earth Planet Sci Lett 195(3):211–221

Chevrel MO, Guilbaud M-N, Siebe C (2016a) The ~AD 1250 effusive eruption of El Metate shield volcano (Michoacán, México): magma source, crustal storage, eruptive dynamics, and lava rheology. Bull Volcanol 78:1–28

Chevrel MO, Siebe C, Guilbaud M-N, Salinas S (2016b) The AD 1250 El Metate shield volcano (Michoacán): Mexico's most voluminous Holocene eruption and its significance for archeology and hazards. The Holocene 26(3):471–488

Connor CB (1987) Structure of the Michoacán-Guanajuato volcanic field, Mexico. J Volcanol Geotherm Res 33:191–200

Connor CB (1990) Cinder cone clustering in the Trans-Mexican Volcanic Belt: implications for structural and petrologic models. J Geophys Res 95(B12):19395–19405

Connor CB, Condit CD, Crumpler LS, Aubele JC (2012) Evidence of regional structural controls on vent distribution: Springerville volcanic field, Arizona. J Geophys Res Solid Earth 97(B9):12349–12359

Conway FM, Connor CB, Hill BE, Condit CD, Mullaney K, Hall CM (1998) Recurrence rates of basaltic volcanism in SP cluster, San Francisco volcanic field, Arizona. Geology 26(7):655–658

Deligne NI, Conrey RM, Cashman KV, Champion DE, Amidon WH (2016) Holocene volcanism of the upper McKenzie River catchment, Central Oregon cascades, USA. Bull Geol Soc Am 128(11/12):1618–1635. https://doi.org/10.1130/B31405.1

Di Traglia F, Morelli S, Casagli N, Garduño-Monroy VH (2014) Semi-automatic delimitation of volcanic edifice boundaries: validation and application to the cinder cones of the Tancitaro–Nueva Italia region (Michoacán–Guanajuato volcanic field, Mexico). Geomorphol 219:152–160

Faugere B (2006) Cueva de los Portales: Un sitio arcaico del norte de Michoacán, México. Colección Científica. CEMCA-INAH, México

Fisher, CT, Leisz, SJ (2013) New perspectives on Purépecha urbanism through the use of LiDAR at the site of Angamuco. In: Comer, D.C., Harrower, M.J. (Eds.) Mapping archaeological landscapes from space. Springer Briefs in Archaeology: 199–210

Fisher RV, Schmincke HU (1984) Pyroclastic rocks. Springer-Verlag, Berlin, p 472

Fisher CT, Cohen AS, Fernández-Diaz JC, Leisz SJ (2017) The application of airborne mapping LiDAR for the documentation of ancient cities and regions in tropical regions. Quat Int 448:129–138

Foshag WF, González-Reyna J (1956) Birth and development of Parícutin volcano, Mexico. US Geol Surv Bull 965D:355–485

Guilbaud MN, Siebe C, Salinas S (2009) Excursions to Paricutin and Jorullo (Michoacán), the youngest volcanoes of the Trans-Mexican Volcanic Belt. A commemorative fieldtrip on the occasion of the 250th anniversary of Volcán Jorullo's birthday on September 29, 1759. Impretei S.A., México, D.F., 31 p

Guilbaud M-N, Siebe C, Layer P, Salinas S, Castro-Govea R, Garduño-Monroy VH, Corvec NL (2011) Geology, geochronology, and tectonic setting of the Jorullo volcano region, Michoacán, México. J Volcanol Geotherm Res 201(1–4):97–112

Guilbaud M-N, Siebe C, Layer P, Salinas S (2012) Reconstruction of the volcanic history of the Tacámbaro-Puruarán area (Michoacán, México) reveals high frequency of Holocene monogenetic eruptions. Bull Volcanol 74(5):1187–1211

Harris AJ, Rowland SK, Villeneuve N, Thordarson T (2017) Pāhoehoe, 'a 'ā, and block lava: an illustrated history of the nomenclature. Bull Volcanol 79(1):7

Hasenaka T (1992) Contrasting volcanism in the Michoacán-Guanajuato volcanic field, Central Mexico: shield volcanoes vs. cinder cones. In: Aoki, K (ed) Subduction volcanism and tectonics of Western Mexican Volcanic Belt: Sendai, Japan, Tohoku University, 248 p

Hasenaka T, Carmichael ISE (1985a) A compilation of location, size, and geomorphological parameters of volcanoes of the Michoacán-Guanajuato volcanic field, Central Mexico. Geofis Int 24:577–607

Hasenaka T, Carmichael ISE (1985b) The cinder cones of Michoacán-Guanajuato, Central Mexico: their age, volume and distribution, and magma discharge rate. J Volcanol Geotherm Res 25:105–124

Hasenaka T, Carmichael ISE (1987) The cinder cones of Michoacán-Guanajuato, Central Mexico: petrology and chemistry. J Petrol 28:241–269

Jerram DA, Martin VM (2008) Understanding crystal populations and their significance through the magma plumbing system. In: Annen

C, Zellmer GF (eds) Dynamics of Crustal Magma Transfer, Storage and Differentiation. Geological Society London Special Publications 304:133-148

Johnson CA, Harrison CGA (1990) Neotectonics in Central Mexico. Phys Earth Planet Inter 64:187–210

Johnson ER, Wallace PJ, Delgado Granados H, Manea VC, Kent AJ, Bindeman IN, Donegan CS (2009) Subduction-related volatile recycling and magma generation beneath Central Mexico: insights from melt inclusions, oxygen isotopes and geodynamic models. J Petrol 50(9):1729–1764

Johnson ER, Wallace PJ, Cashman KV, Granados HD (2010) Degassing of volatiles (H_2O, CO_2, S, Cl) during ascent, crystallization, and eruption at mafic monogenetic volcanoes in Central Mexico. J Volcanol Geotherm Res 197(1–4):225–238

Juárez-Arriaga E, Böhnel H, Carrasco-Núñez G, Mahgoub AN (2018) Paleomagnetism of Holocene lava flows from Los Humeros caldera, eastern Mexico: discrimination of volcanic eruptions and their age dating. J S Am Earth Sci 88:736–748

Kim Y, Miller MS, Pearce F, Clayton RW (2012) Seismic imaging of the Cocos plate subduction zone system in Central Mexico. Geochem Geophys Geosyst 13(7):Q07001. https://doi.org/10.1029/2012GC004033

Kshirsagar P, Siebe C, Guilbaud M-N, Salinas S, Layer PW (2015) Late Pleistocene Alberca de Guadalupe maar volcano (Zacapu basin, Michoacán): stratigraphy, tectonic setting, and paleohydrogeological environment. J Volcanol Geotherm Res 304: 214–236. https://doi.org/10.1016/j.jvolgeores.2015.09.003

Kshirsagar P, Siebe C, Guilbaud MN, Salinas S (2016) Geological and environmental controls on the change of eruptive style (phreatomagmatic to Strombolian-effusive) of Late Pleistocene El Caracol tuff cone and its comparison with adjacent volcanoes around the Zacapu basin (Michoacán, México). J Volcanol Geotherm Res 318:114–133. https://doi.org/10.1016/j.jvolgeores.2016.03.015

Larrea P, Salinas S, Widom E, Siebe C, Abbitt RJF (2017) Compositional and volumetric development of a monogenetic lava flow field: the historical case of Paricutin (Michoacan, Mexico). J Volcanol Geotherm Res 348:36–48

Larrea P, Widom E, Siebe C, Salinas S, Kuentz D (2019) A re-interpretation of the petrogenesis of Paricutin volcano: distinguishing crustal contamination from mantle heterogeneity. Chem Geol 504:66–82. https://doi.org/10.1016/j.chemgeo.2018.10.026

Le Bas M, Maitre RL, Streckeisen A, Zanettin B (1986) IUGS subcommission on the systematics of igneous rocks. A chemical classification of volcanic rocks based on the total alkali-silica diagram. J Petrol 27(3):745–750

Le Corvec N, Spörl KB, Rowland J, Lindsay J (2013) Spatial distribution and alignments of volcanic centers: clues to the formation of monogenetic volcanic fields. Earth Sci Rev 124:96–114

Leonhardt R, Heunemann C, Krasa D (2004) Analyzing absolute paleointensity determinations: acceptance criteria and the software ThellierTool4.0. G-cubed 5:1–11. https://doi.org/10.1029/2004GC000807

Lipman PW, Banks NG (1987) AA flow dynamics, Mauna Loa 1984. US Geol Surv Prof Pap 1350:1527–1567

Luhr JF, Simkin T (1993) Paricutin: the volcano born in a Mexican cornfield. Geoscience Press, 427 pp

Mahgoub AN, Böhnel H, Siebe C, Salinas S, Guilbaud M-N (2017a) Paleomagnetically inferred ages of a cluster of Holocene monogenetic eruptions in the Tacámbaro-Puruarán area (Michoacán, México): implications for volcanic hazards. J Volcanol Geotherm Res 347:360–370. https://doi.org/10.1016/j.jvolgeores.2017.10.004

Mahgoub AN, Böhnel H, Siebe C, Chevrel MO (2017b) Paleomagnetic study of El Metate shield volcano (Michoacán, Mexico) confirms its monogenetic nature and young age (~AD 1250). J Volcanol Geotherm Res 336:209–218. https://doi.org/10.1016/j.jvolgeores.2017.02.024

Mahgoub AN, Reyes-Guzmán N, Böhnel H, Siebe C, Pereira G, Dorison A (2018) Paleomagnetic constraints on the ages of the Holocene Malpaís de Zacapu lava flow eruptions, Michoacán (Mexico): implications for archeology and volcanic hazards. The Holocene 28(2): 229–245

Mahgoub AN, Juárez-Arriaga E, Böhnel H, Siebe C, Pavón-Carrasco FJ (2019) Late-Quaternary secular variation data from Mexican volcanoes. Earth Planet Sci Lett 519:28–39

Martí J, López C, Bartolini S, Becerril L, Geyer A (2016) Stress controls of monogenetic volcanism: a review. Front Earth Sci 4:1–17

Michelet D (1993) El Centro-Norte de Michoacán: características generales de su estudio regional. In: Michelet D (ed) El Proyecto Michoacán 1983–1987. Medio ambiente e introducción a los trabajos arqueológicos. CEMCA, México, pp 9–52

Michelet D (1998) Topografía y prospección sistemática de los grandes asentamientos del Malpaís de Zacapu: claves para un acercamiento a las realidades sociopolíticas. In: Darras V (ed) Génesis, culturas y espacios en Michoacán. CEMCA, México, pp 47–59. https://doi.org/10.4000/books.cemca.3396

Morelli S, Monroy VH, Gigli G, Falorni G, Rocha EA, Casagli N (2010) The Tancitaro debris avalanche: characterization, propagation and modeling. J Volcanol Geotherm Res 193(1–2):93–105

Nolan ML (1979) Impact of Paricutin on five communities. In: Sheets PD, Grayson DK (eds) Volcanic activity and human ecology. Academic Press, New York, pp 293–338

O'Reilly W (1984) Rock and mineral magnetism. Chapman and Hall, 220 pp

Ownby S, Granados HD, Lange RA, Hall CM (2007) Volcán Tancítaro, Michoacán, Mexico, 40 Ar/39 Ar constraints on its history of sector collapse. J Volcanol Geotherm Res 161(1):1–14

Ownby SE, Lange RA, Hall CM, Delgado-Granados H (2011) Origin of andesite in the deep crust and eruption rates in the Tancítaro–Nueva Italia region of the central Mexican arc. Geol Soc Am Bull 123(1–2):274–294

Pacheco JF, Valdés-González C, Delgado-Granados H, Singh SK, Zúñiga R, Mortera-Gutiérrez CA, Santoyo MA, Domínguez J, Barrón R (1999) Tectonic implications of the earthquake swarm of 1997 in the Michoacán triangle, Mexico. J S Am Earth Sci 12:567–577

Parfitt EA, Wilson L (1995) Explosive volcanic eruptions-IX. The transition between Hawaiian-style lava fountaining and Strombolian explosive activity. Geophys J Int 121(1):226–232

Pavón-Carrasco FJ, Osete ML, Torta JM, De Santis A (2014) A geomagnetic field model for the Holocene based on archaeomagnetic and lava flow data. Earth Planet Sci Lett 388:98–109. https://doi.org/10.1016/j.epsl.2013.11.046

Pereira G, Padilla-Gutiérrez EF (2018) La Ciudad Perdida. Raíces de los Soberanos Tarascos. Ediciones del Museo Nacional de Antropología, Co-edición INAH/CEMCA, México, 122 p. ISBN-978-607-539-117-5

Pérez-López R, Legrand D, Garduño-Monroy VH, Rodríquez-Pascua MA, Giner-Robles JL (2011) Scaling laws of the size-distribution of monogenetic volcanoes within the Michoacán-Guajajuato volcanic field (Mexico). J Volcanol Geotherm Res 201:65–72

Pinkerton H, Wilson L (1994) Factors controlling the lengths of channel-fed lava flows. Bull Volcanol 56(2):108–120

Pola A, Macías JL, Garduño-Monroy VH, Osorio-Ocampo S, Cardona-Melchor S (2014) Successive collapses of the el Estribo volcanic complex in the Pátzcuaro Lake, Michoacán, Mexico. J Volcanol Geotherm Res 289:41–50

Polacci M, Papale P (1997) The evolution of lava flows from ephemeral vents at Mount Etna: insights from vesicle distribution and morphological studies. J Volcanol Geotherm Res 76(1–2):1–17

Pollard HP (1993) Tariácuri's legacy. The Prehispanic Tarascan state. University of Oklahoma press, Norman

Pollard HP (2011) Una larga caminata: el análisis regional dentro de la arqueología tarasca. In: Williams E, Weigand PC (eds) Patrones de asentamiento y actividades de subsistencia en el Occidente de México. Zamora, Colegio de Michoacán, pp 21–34

Punzo-Díaz JL, Martínez-Vázquez DB (2018) La Cueva de los Hacheros: Un probable sitio del Pleistoceno Tardío y Holoceno Temprano, Michoacán, México. Arqueología Iberoamericana 40:3–8

Ramírez-Uribe I (2017) Geología y aspectos arqueológicos del volcán monogenético Rancho Seco y estructuras volcánicas vecinas (Michoacán, México). Bachelor Thesis, Ciudad de México, Universidad Nacional Autónoma de México, p 31

Rasoazanamparany C, Widom E, Siebe C, Guilbaud M-N, Spicuzza MJ, Valley JW, Valdez G, Salinas S (2016) Temporal and compositional evolution of Jorullo volcano, Mexico: implications for magmatic processes associated with a monogenetic eruption. Chem Geol 434:62–80

Rees JD (1979) Effects of the eruption of Paricutin volcano on landforms, vegetation, and human occupancy. In: Sheets PD, Grayson DK (eds) Volcanic activity and human ecology. Academic Press, New York, pp 249–292

Reyes-Guzmán N, Siebe C, Chevrel MO, Guilbaud MN, Salinas S, Layer P (2018) Geology and radiometric dating of quaternary monogenetic volcanism in the western Zacapu lacustrine basin (Michoacán, México): implications for archaeology and future hazard evaluations. Bull Volcanol 80:18

Rowland SK, Jurado-Chichay Z, Ernst G, Walker GP (2009) Pyroclastic deposits and lava flows from the 1759–1774 eruption of El Jorullo, Mexico: Aspects of 'violent Strombolian'activity and comparison with Parícutin. Studies in Volcanology: the Legacy of George Walker. IAVCEI, Special Publications 2:105–28.

Siebe C, Guilbaud M-N, Salinas S, Kshirsagar P, Chevrel MO, De la Fuente JR, Hernández-Jiménez A, Godínez L (2014) Monogenetic volcanism of the Michoacán-Guanajuato volcanic field: Maar craters of the Zacapu basin and domes, shields, and scoria cones of the Tarascan highland (Paracho-Paricutin region). In: Field guide, Pre-meeting Fieldtrip for the 5th International Maar Conference (5IMC-IAVCEI). Querétaro, 13–17 November, 33 pp

Siebe C, Reyes N, Guilbaud MN, Salinas S, Mahgoub AN, Böhnel H, Chevrel OM, Kshirsagar PV, Larrea P (2018) Historia del vulcanismo reciente en Michoacán y sus implicaciones para los asentamientos humanos. Coloquio internacional: movilidades, territorios y cambios sociopolíticos en el centro-oeste de México. Museo Nacional de Antropología, Ciudad de México, Mexico, April 23-25 2018, Abstracts, p. 3-5

Smith IEM, Németh K (2017) Source to surface model of monogenetic volcanism: a critical review. Geol Soc Lond Spec Publ 446:1–28

Tauxe L, Staudigel H (2004) Strength of the geomagnetic field in the cretaceous normal superchron: new data from submarine basaltic glass of the Troodos ophiolite. Gcubed 5:1–16. https://doi.org/10.1029/2003GC000635

Valentine GA, Connor CB (2015) Basaltic volcanic fields. In: Sigurdsson H, Houghton BF, McNutt S, Rymer H, Stix J (Eds) The Encyclopedia of Volcanoes (2nd Edition), pp. 423-439

Verma SP, Hasenaka T (2004) Sr, Nd, and Pb isotopic and trace element geochemical constraints for a veined-mantle source of magmas in the Michoacan-Guanajuato volcanic field, west-central Mexican volcanic belt. Geochem J 38(1):43–65

Watts WA, Bradbury JP (1982) Paleoecological studies at Lake Patzcuaro on the west-central Mexican Plateau and at Chalco in the Basin of Mexico. Quat Res 17(1):56–70

Yu Y, Dunlop DJ, Özdemir Ö, Ueno H (2001) Magnetic properties of Kurokami pumices from Mt. Sakurajima, Japan. Earth Planet Sci Lett 192(3):439–446